Construction of multi-stimuli responsive highly porous switchable frameworks by *in-situ* solid-state generation of spiropyran switches

Jinyu Sheng[+], Jacopo Perego[+], Silvia Bracco, Włodzimierz Czepa, Wojciech Danowski,* Simon Krause, Piero Sozzani, Artur Ciesielski, Angiolina Comotti,* Ben. L. Feringa*

Dr. J. Sheng, Dr. W. Danowski, Dr. S. Krause, Prof. B. L. Feringa
Stratingh Institute for Chemistry, University of Groningen, Groningen, the Netherlands. Nijenborgh 4, 9747 AG, Groningen, The Netherlands.
Email: danowski@unistra.fr; b.l.feringa@ rug.nl.

Dr. J. Perego, Prof. S. Bracco, prof. P. Sozzani, prof. A. Comotti
Email: angiolina.comotti@unimib.it
Department of Materials Science, University of Milano Bicocca, Milan, Italy. Via R. Cozzi 55, Milan 20125, Italy

W. Czepa
Faculty of Chemistry, Adam Mickiewicz University, Uniwersytetu Poznańskiego 8, 61614 Poznań, Poland.

W. Czepa, Prof. A. Ciesielski
Center for Advanced Technologies, Adam Mickiewicz University, Uniwersytetu Poznańskiego 10, 61614 Poznań, Poland.

Dr. W. Danowski, Prof. A. Ciesielski
Université de Strasbourg, CNRS, ISIS, 8 allée Gaspard Monge, 67000 Strasbourg, France.

Dr. S. Krause
Max Planck Institute for Solid State Research, Heisenbergstr. 1, 70569 Stuttgart, Germany

[+] These authors contributed equally to this work.

Keywords: photoswitch, porous aromatic framework, porous material, smart material, multi-stimuli responsiveness, spiropyran, solid-state isomerization.

Abstract: Stimuli-responsive molecular systems supported within permanently porous materials offer the opportunity to host dynamic functions operating multifunctional smart materials. However, the construction of highly porous frameworks featuring external-stimuli responsiveness, for example by light excitation, is still in its infancy. Here we present a general strategy to construct spiropyran-functionalized highly porous switchable aromatic frameworks (PSFs) by modular and high-precision anchoring of molecular hooks and an innovative *in-situ* solid-state grafting approach. Three spiropyran-grafted frameworks bearing distinct functional groups exhibiting various stimuli-responsiveness were generated by two-step post-solid-state synthesis of a parent indole-based material. The quantitative transformation and preservation of high porosity were demonstrated by spectroscopic and gas adsorption techniques. For the first time, we provide a highly efficient strategy to construct multi-stimuli-responsive, yet structurally robust, spiropyran materials with high pore capacity which was proved essential for the reversible and quantitative isomerization in the bulk as demonstrated by solid-state NMR spectroscopy. The overall strategy allowed to construct dynamic materials which undergo reversible transformation of spiropyran to zwitterionic merocyanine, by chemical and physical stimulation, showing potential for pH active control, responsive gas uptake and release, contaminant removal, and water harvesting.

Introduction

Stimuli-responsive molecules[1–3] offer great opportunities as building blocks for the construction of adaptive materials capable of undergoing reversible conformational changes under the effect of external physical or chemical stimuli.[4–10] In this context, spiropyrans (SPs)[11–13] are among the most prolific representatives of molecular switches due to their prominent multi-stimuli responsiveness encompassing light, mechanical force, pH, temperature, polarity of media, metal ions and redox potential.[11,14,15] The isomerization from cyclized nonpolar form to zwitterionic conjugated merocyanine (MC) form induces drastic changes in both molecular structure and physicochemical properties.[12,15–17] In addition, a careful choice of substituents allows for the regulation of thermal stability of the MC form, the absorption wavelength and their photostability as well as the robustness to hydrolysis.[14,17] Due to these versatile features, SPs were widely used for construction of responsive materials including polymers,[17–19] gels,[20–23] thin films[24] or monolayers,[25,26] small-molecule assemblies,[27,28] biohybrid system[29] and porous materials.[30–39] The development of porous solids capable of reversibly interconverting between two or more states in response to one or more stimuli offers opportunities to manipulate noninvasively the properties of the material enabling new functions with the advantage of broad flexibility with the choice of the applied stimulus. In this context, the incorporation of SPs into porous systems offers a general and convenient approach to develop multi-stimuli responsive porous materials for applications ranging from cargo capture, delivery and release to chemical sensing.[13,40]

Pioneering studies by Klajn and coworkers on the incorporation of SPs in nanoporous materials indicated the partially-preserved multi-stimuli responsiveness of the SP-moiety with respect to that in solution.[30] Recently, major attention was focused on the incorporation of SPs as guests or pendant moieties in metal-organic frameworks (MOFs) proving a suitable strategy to achieve fast photoisomerization,[31] modulation of conductivity,[33–35] capability of water desalination[36] and tuning of gas adsorption.[41,42] However, the effective integration of SPs in highly porous covalent frameworks and the preservation of their isomerization behavior remains a major challenge.[43] In addition, the fabrication of SP-functionalized porous switchable frameworks with large accessible surface areas is unexplored. A typical strategy to construct highly porous materials is to exploit the efficient Yamamoto Ullmann-type coupling reaction, which unlike Suzuki-type coupling, forms highly porous aromatic frameworks (PAFs) with unparalleled surface areas.[44,45] By contrast, as a result of high reactivity of the Ni(0) complex, the number of the functional groups tolerated in these reactions are severely limited. Hence, apart from rare examples of overcrowded alkenes,[46,47] molecular switches are largely incompatible with the Yamamoto coupling reaction, consequently compromising the fabrication methods of switchable aromatic frameworks.

Here, we provide a judicious post-synthetic strategy for the construction of SP-grafted highly porous switchable frameworks (**SP-PSFs**). We exploit *in-situ* solid-state synthesis of the SPs moieties in the pores of the framework via a pre-anchored indole precursor inside a porous aromatic frameworks (PAF) followed by methylation of the indole and finally the grafting of the SP moiety by condensation of the

indoline Fisher-base with a variety of salicylaldehydes. This approach bypasses the limited functional group-tolerance of Yamamoto coupling as a result of the high stability of indole moiety and allows for fabrication of materials decorated with SP moieties exhibiting BET surface area as high as 1608 m^2g^{-1} and 1.21 cm^3g^{-1} total pore volume. Due to the modularity and high precision of this approach, three novel **SP-PSFs** with distinct properties and functions were fabricated illustrating the scope and versatility of SP switches. In addition to the high porosity, all the synthesized porous materials possess multi-stimuli responsiveness comparable to that of the SPs in solution, owing to the high porosity minimizing the interactions of the responsive moieties with the aromatic framework. These highly porous and responsive materials were tested for various applications, including acidic gas adsorption and detection, as well as removal of metal ion from solution (Figure 1).

Figure 1. Schematic representation of *in situ* generation of SP switches and their transformations in PSFs. Formation of **Indole-PAF** by direct insertion of indole moieties covalently connected to the framework (**Indole-PAF**), followed by post-synthetic modification of the indole moiety and i*n-situ* generation of the SP switch in the framework **(SP-PSFs)**, and responsive behavior of SP switch group triggered by different stimuli to form **MC-PSF** (from left to right).

Results and discussion

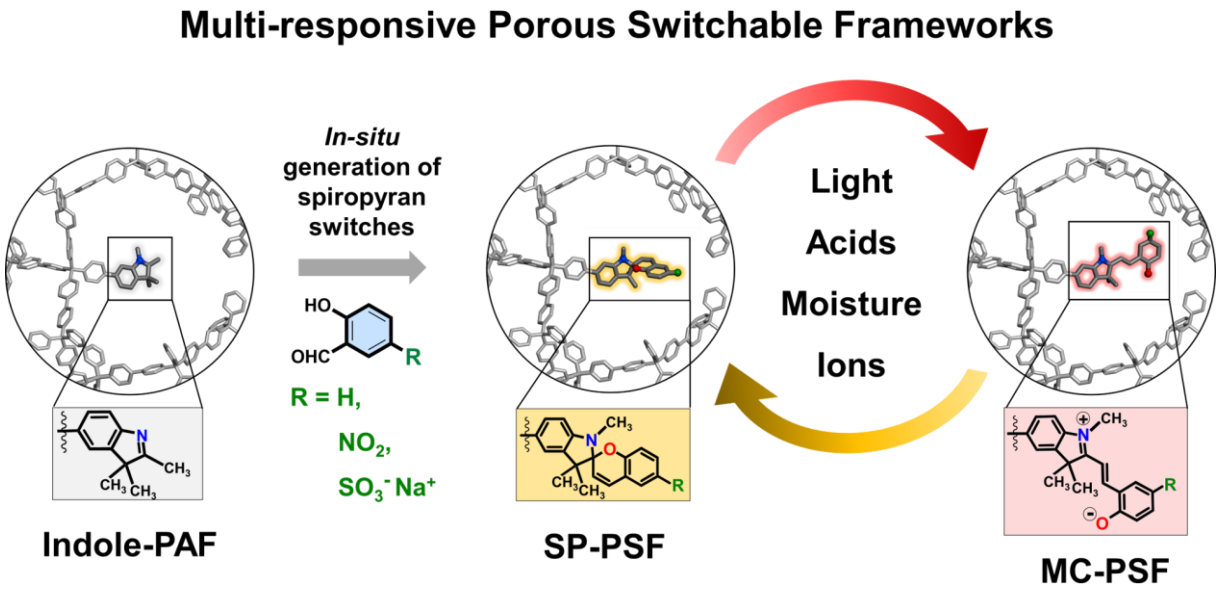

Synthesis and characterization of PAFs and NSP-PSF. The parent indole-grafted porous aromatic framework (**indole-PAF**) was synthesized by a Yamamoto-Ullmann cross-coupling reaction. Since monofunctional or linear co-monomers are expected to drastically decrease the porosity of the frameworks,[46,48] here a tritopic indole-appended building block (**1-Br$_3$**) was designed. The indole-bearing monomer was copolymerized with a porogenic tetra-*p*-bromo-phenylmethane (**TPM-Br$_4$**) monomer in 1:4 (**1-Br$_3$** : **TPM-Br$_4$**) molar ratio (Figure 2a). The copolymerization of tetratopic and di- or tritopic monomers by Yamamoto coupling is recognized for yielding materials with reduced surface area in comparison to the frameworks constructed exclusively from the tetratopic monomers. With the expectation that a higher porosity would facilitate subsequent polymerization reactions inside the pore space while still preventing the tight packing of the spiropyrans[17], the 4:1 proportion of porogenic and functional monomers was selected to balance the porosity of the materials and the concentration of

indole moieties in the framework. As fabricated **indole-PAF** material exhibits high pore capacity as established by N_2 adsorption measurements at 77 K. A typical type IV isotherm with large hysteresis is observed for this material (Figure 2b, grey) indicating the presence of micropores and expanded capacity in the mesopore region at high gas loading. The Langmuir and Brunauer–Emmett–Teller (BET) surface areas were as large as 1913 and 1708 m^2g^{-1}, respectively. The pore-size distribution was calculated using non-local density functional theory (NL-DFT), which indicated that micropores constitute ca. 32% of pore volume, with the total pore volume of 1.26 cm^3g^{-1}, highlighting significant tendency of the material to generate mesopores. Subsequent N-methylation of **indole-PAF** with methyl iodide afforded **indolium-PAF** (Figure 2a) with reduced BET surface area and total pore volume to 1310 m^2g^{-1} and 0.81 cm^3g^{-1}, respectively. Such a significant drop in the available voids is expected given the presence of bulky iodide anions in the structure, as confirmed by energy-dispersive X-ray spectroscopy (EDS) (Figure S34). Interestingly, while the microporosity dropped from 0.54 $cm^3\ g^{-1}$ to 0.44 $cm^3\ g^{-1}$ (percentage decrease = 18%), the mesoporosity was more affected with a 48% decrease of mesopore volume. Subsequent condensation of **iodolium-PAF** with 5-nitro-salicylaldehyde in the presence of base yielded a nitro-appended spiropyran porous switchable framework (**NSP-PSF)**. The **NSP-PSF** material exhibits higher porosity than the preceding **indolium-PAF** with BET surface area and total pore volume of 1606 $m^2\ g^{-1}$ and 1.08 $cm^3\ g^{-1}$, respectively (Table S1, see SI section 4.1 for the discussion on the impact of changes in molecular weight of the monomeric units on the porosity of the framework), which is consistent with removal of the loosely-bound bulky iodides from the pores of the framework. The lower BET surface area of the **NSP-PSF** with respect to the parent **indole-PAF** framework is in accordance with the formation of the SP pendants, which are bulkier and heavier than the indole moieties, thus occupying more volume in the material and leading to the increase of the molecular weight of the monomeric unit.

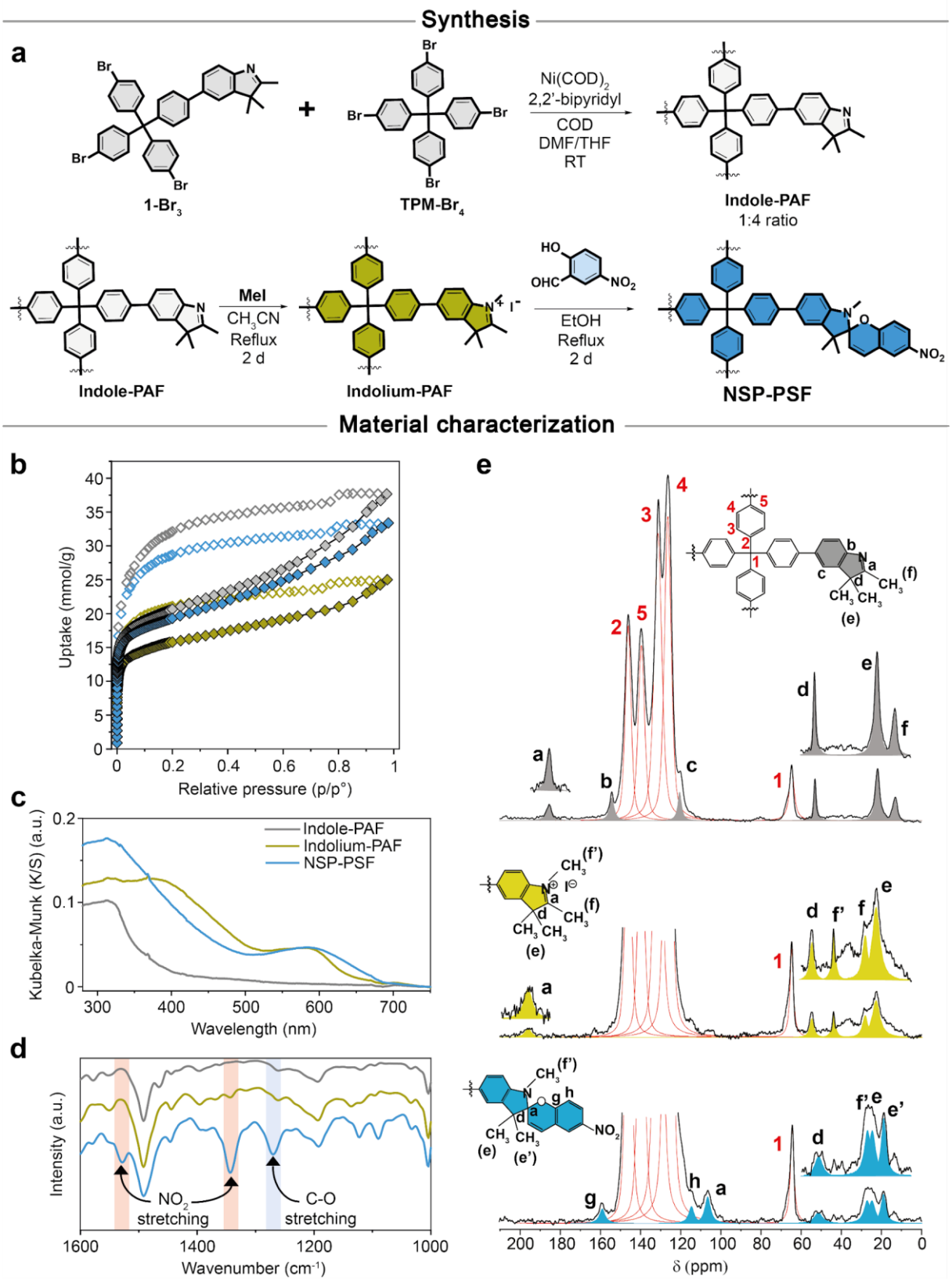

Figure 2. a. Top: synthesis of **indole-PAF** using Yamamoto-Ullmann cross-coupling reaction; bottom: post-synthetic functionalization to yield SP grafted porous switchable framework with nitro functional groups (**NSP-PSF)**. **b.** Nitrogen adsorption isotherms collected at 77 K of **indole-PAF** (grey), **indolium-PAF** (yellow) and **NSP-PSF** (blue). **c.** Kubelka-Munk transformed DR UV/Vis spectra of **indole-PAF**, **indolium-PAF** and **NSP-PSF**. **d.** DRIFT-IR spectra of **indole-PAF**, **indolium-PAF** and **NSP-PSF**. **e.** $^{13}C\{^{1}H\}$ CP MAS spectra of **indole-PAF** (top), **indolium-PAF** (medium) and **NSP-PSF** (bottom) materials performed at 298 K at a spinning speed of 12.5 kHz with a contact time of 2 ms. The spectra were simulated

by Lorentzian line-shape functions. The spectra are magnified 2-3 times in the regions 200 - 175 ppm and 60 - 5 ppm to highlight indole, indolium and SP typical ^{13}C NMR signals.

These solid-state functionality transformations were further confirmed by diffuse-reflectance UV/Vis (DR UV/Vis) and diffuse-reflectance infrared Fourier Transform (DRIFT) spectroscopies. The **NSP-PSF** material showed a clearly distinguishable spectrum compared to the predecessor material **indolium-PAF** and parent material **indole-PAF** (Figure 2c), indicating the step-wise transformation of functional groups during the post-synthetic solid-state transformations within the solid framework. DRIFT spectroscopy displays the appearance of two additional intense bands for **NSP-PSF** material centered at 1530 cm^{-1} and 1340 cm^{-1} associated with the asymmetric and symmetric stretching of the nitro- group (Figure 2d), respectively. The two additional bands around 1100 cm^{-1} (Figure 2d, blue spectrum) were ascribed to the C-H out of plane asymmetric bending modes.[49] Together with a C_{spiro}-O stretching bands centered at 1260 cm^{-1}, the combined data strongly support the successful formation of the **NSP** moiety.[50] Furthermore, the presence of characteristic ^{13}C resonances in ^{13}C CP MAS NMR allowed to unambiguously confirm the chemical structures of the framework at each stage of the solid-state synthesis (Figure 2e, Table S2-S7 and Figure S29 for the comparison of ss ^{13}C CP MAS NMR of indole-PAF with monomers).[51] The formation of **indolium-PAF** was supported by the presence of a signal at 43.8 ppm characteristic of methyl group adjacent to charged quaternary nitrogen (CH_3-N^+) moiety (Figure 2e, middle spectrum). Accordingly, the disappearance of the resonance at 196.0 ppm ascribed to the iodolium carbon in 2-position (C_a, see Figure 2e, middle panel) and emergence of the resonance at 106.7 ppm characteristic of quaternary spiro carbon (C_a, Figure 2e, bottom panel) along with two distinct resonances for diastereotopic methyl groups (e and e') indicated the successful conversion to spiropyran derivative (**NSP-PSF**) (Figure 2e, bottom spectrum). Importantly, characteristic shifts of the diagnostic "C_a" resonance (Figure 2e, see SI section 4.2 for further discussion) in the ^{13}C CP MAS NMR spectra showed quantitative conversion, within the sensitivity limit of the technique, at each stage of the transformation, indicating the remarkably high efficiency of this approach. These results support the fact that the reaction does not generate side products and residues which are irreversibly encapsulated within the pores. The exceptionally high efficiency of this solid-state SP synthesis most likely stems from the high porosity of the material and its hierarchical micro-/meso-porous structure which facilitates mass transport through the solid during the whole process. It should be emphasized that this post-solid-state synthesis strategy successfully proved the formation of **NSP-PSF** materials not accessible via direct synthetic methods. Thermal gravimetric analysis (TGA) revealed the high thermal stability of these porous materials, an initial weight loss is observed above 300°C due to the decomposition of the SP moiety, while the framework is stable up to 450°C (Figure S36). Powder X-ray diffraction (PXRD) data confirmed the amorphous nature of the materials (Figure S38) and scanning electron microscopy (SEM) images (Figure S39-41) showed that the porous materials comprise aggregates of submicrometer-size particles, common for the frameworks formed via irreversible reactions.

Extension of strategy for the synthesis of SP-PSF and SSP-PSF materials. SP motifs with various substituents at 6-position of the benzopyran part show dramatic differences in properties, leading to a variety of functions such as photoacidity,[52–54] actuation[18,20,23,55] and multi-stimuli responsiveness.[30,56,57] Therefore, we further extended the generality of our strategy to the fabrication of non-substituted and sulfonated SP functionalized materials (denoted as **SP-PSF** and **SSP-PSF**, respectively). By the condensation reaction of salicylaldehyde or sodium salicylaldehyde-5-sulfonate with **indolium-PAF**, we successfully constructed **SP-PSF** and **SSP-PSF** materials (Figure 3a)**,** respectively. These two materials showed similar features as their sister **NSP-PSF** counterpart as both materials maintained high BET surface areas and pore volume of 1608 $m^2 g^{-1}$ and 1.21 $cm^3 g^{-1}$ for **SP-PSF** and 1440 m^2g^{-1} and 0.76 $cm^3 g^{-1}$ for **SSP-PSF**, respectively (Figure 3b). At higher partial pressure, both materials considerably differ regarding the polarity of the framework: the less polar **SP-PSF** displays a swelling behavior,[58] as confirmed by the wide hysteresis in the desorption curve upon nitrogen adsorption at 77 K, **SSP-PSF** showed much lower uptake and narrower hysteresis loop between adsorption-desorption branches (Figure 3b). Indeed, CO_2 adsorption isotherms collected at 195 K show a comparable behavior owing to stronger interactions of CO_2 with the frameworks which induce similar pore expansion in both frameworks, indicating that the swellability of these **PSFs** strongly depends on the polarity of the environment and adsorbate (Figure 3b, inset, see Figure S27 and discussion therein). DR UV/Vis spectra of both materials indicate that the responsive pendants are initially in the cyclized SP form as no bands characteristic of the opened MC moieties were observed in the visible region of the spectra (Figure 3c). In both cases, clear C_{spiro}-O bond stretching bands were observed at 1260 cm^{-1} in the DRIFT spectra, indicating the successful grafting of the SP motifs in the materials (Figure 3d). An additional band at ~1095 cm^{-1} characteristic of the SO_3^- group was observed in **SSP-PSF**, indicating the successful construction of the sulfonated spiropyran (Figure 3d, pink spectrum).[35,59] Furthermore, in the case of **SSP-PSF**, EDS spectroscopy proved the presence of both sulfur and sodium elements in the material with concomitant absence of iodine (Figure S35), indicating the complete transformation of functionalities. Finally, ^{13}C CP MAS NMR spectroscopy demonstrates the quantitative transformation of functionalities, within the sensitivity of the analysis (Figure S31). SEM images and PXRD (Figure S42-43 and S38) confirm that both **SP-PSF** and **SSP-PSF** materials have a similar morphology and are amorphous in nature.

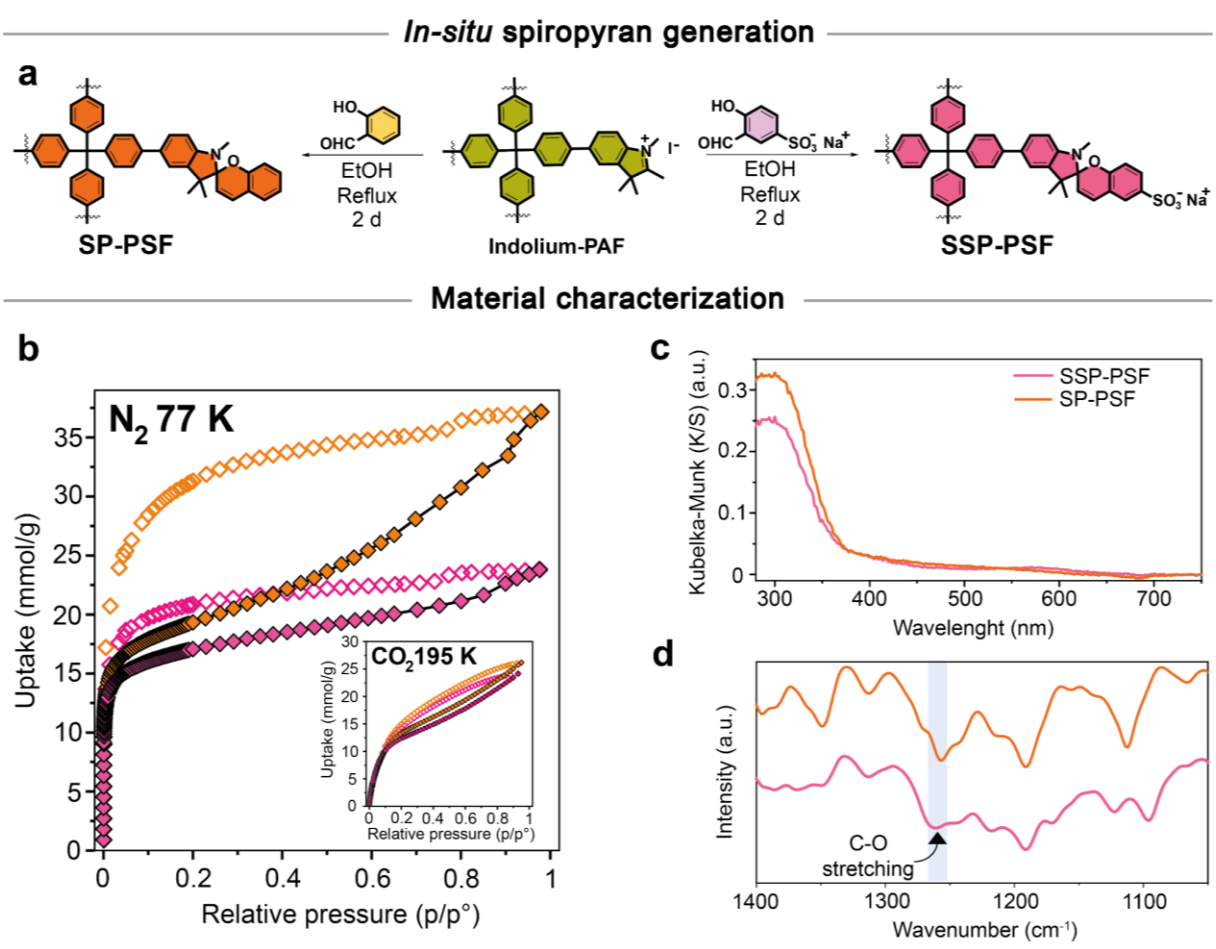

Figure 3. a. Extension of strategy to the synthesis of the **SP-PSF** (left) and **SSP-PSF** (right). **b.** Nitrogen adsorption isotherms collected at 77 K of **SP-PSF** (orange) and **SSP-PSF** (pink). **inset.** Carbon dioxide adsorption isotherms collected at 195 K of **SP-PSF** (orange) and **SSP-PSF** (pink). **c.** Kubelka-Munk transformed DR UV/Vis spectra of **SP-PSF** (orange) and **SSP-PSF** (pink). **d.** DRIFT-IR spectra of **SP-PSF** (orange) and **SSP-PSF** (pink).

Stimuli-induced isomerization of SP-PSFs in the solid state.

The photochemical isomerization behavior of the solid **NSP-PSF** material was studied by DRUV/Vis and DRIFT spectroscopies (see Fig. S4-8 for the studies of NSP in solution). The initial DRUV/Vis spectrum (Figure 4b, blue spectrum) showed a small absorption band centered at 600 nm which was ascribed to a small amount of opened MC form present in the pristine sample of **NSP-PSF** material. Upon the irradiation of the material at 365 nm light for 10 s, a dramatic color change from grey to bright blue was observed (Figure 4a), in line with the isomerization of closed SP form to opened MC form via C_{spiro}-O bond cleavage. This change was accompanied by the drastic increase of the intensity of the broad band centered at 600 nm, characteristic of the open MC-form (Figure 4b, green spectrum). Subsequent illumination at 617 nm for 15 min led to the recovery of the initial spectrum (Figure 4b, light blue spectrum), in line with the reversible photoisomerization between the two forms. DRIFT spectroscopy further confirms the isomerization behavior of **NSP-PSF** (Figure S45 and S46). The reversible changes in the DRIFT spectra were observed around ~1260 cm^{-1} upon consecutive UV and Visible light irradiation which can be ascribed to the scission/reformation of C_{spiro}-O bond,[33] further

corroborating the isomerization between closed and open forms. Like the NSP photoisomerization behavior in solution (Figure S6 and S8), the MC form in the solid state was found to be thermally unstable, and a fast equilibration of the MC to SP form was observed at ambient temperature (Figure S51a). The kinetics of the thermal isomerization of the NMC was followed by DRUV/Vis spectroscopy and found to be almost completed within a few hours at ambient temperature. (Figure S51b).

Similar to the typical 6-*H* SP behavior in solution, the **SP-PSF** material does not show any photo-response under ambient conditions due to the low thermal stability of 6-*H* MC form that quickly thermalizes back to the SP form.[60] Instead, the switching behavior of **SP-PSF** material could be triggered upon spontaneous isomerization to the protonated merocyanine (**MCH$^+$-PSF**) by exposure to gaseous or an aqueous HCl solution (1M). An obvious color change from grey to orange could be observed by the naked eye (Figure 4c), indicative of the formation of MCH$^+$. DRUV/Vis and DRIFT spectroscopies indicate that illumination of the **MCH$^+$-PSF** material at 365 nm or in the visible light region leads to the recovery of **SP-PSF** (Figure 4d, and Figure S32), likely with concomitant expulsion of the volatile acid from the framework. This behavior differs from the one in solution as 6-*H* spiropyrans typically open to Z-MCH$^+$ upon protonation and isomerize to E-MCH$^+$ upon irradiation at 365 nm (see Fig. S12-14). Further experiments proved that the **SP-PSF** material could be also regenerated from **MCH$^+$-PSF** in either vacuum or upon heating conditions, which is consistent with the volatility of hydrochloric acid (Figure S54). This pH-responsive behavior was also observed for the **SSP-PSF** material upon treatment with gaseous $HCl_{(g)}$ (Figure S53).

In addition to the pH-responsive behavior, the **SSP-PSF** material shows humidity-induced isomerization. This unique property stems from the SSP pendant, which is known to be stable in the opened MC form in aqueous media in the dark (see Fig. S17-21 for studies in solutions).[61] After storing under ambient conditions in a sealed vial in the dark for 4 weeks, the greyish **SSP-PSF** material changed color to purple, indicating isomerization of the **SSP** pendants (Figure 4e). DRUV/Vis and DRIFT spectra supported the isomerization from SP to MC form in the solid state (Figure 4f, violet UV-Vis spectrum), both showing features characteristic of the MC isomer.[35] Due to the presence of the polar sulfonate side group in the material, moisture under ambient condition may enter the pores of the framework resulting in the increase of the polarity of the environment and therefore leading to the shift in the position of the SP/MC thermal equilibrium in favor of the stabilization of the SMC isomer. Indeed, after soaking of **SSP-PSF** in water, the ^{13}C CP MAS spectrum showed the complete disappearance of the signal at 106.6 ppm of C_{spiro}-O (closed form) and the emergence of two new signals at 196.9 ppm and 183.9 ppm revealing the formation of both ***Z*** and ***E*** isomers of SMC**,** respectively (Figure S33). However, upon thermal treatment and water removal, only the *Z*-SMC reversed back quantitatively to SSP owing to the arrangement of the *Z*-SMC isomer which favour the formation of the closed form (Figure S33). Nevertheless, the N_2 adsorption isotherms collected at 77 K of SSP-PSF in its pristine state and after

water soaking and another activation cycle were almost superimposable, indicating the reversibility of the water uptake without structural changes of the porous material (Fig. S28). This unique behavior of **SSP-PSF** may have potential applications in modulation of proton conductivity,[35] water-harvesting and purification or water-sensing.[62–65]

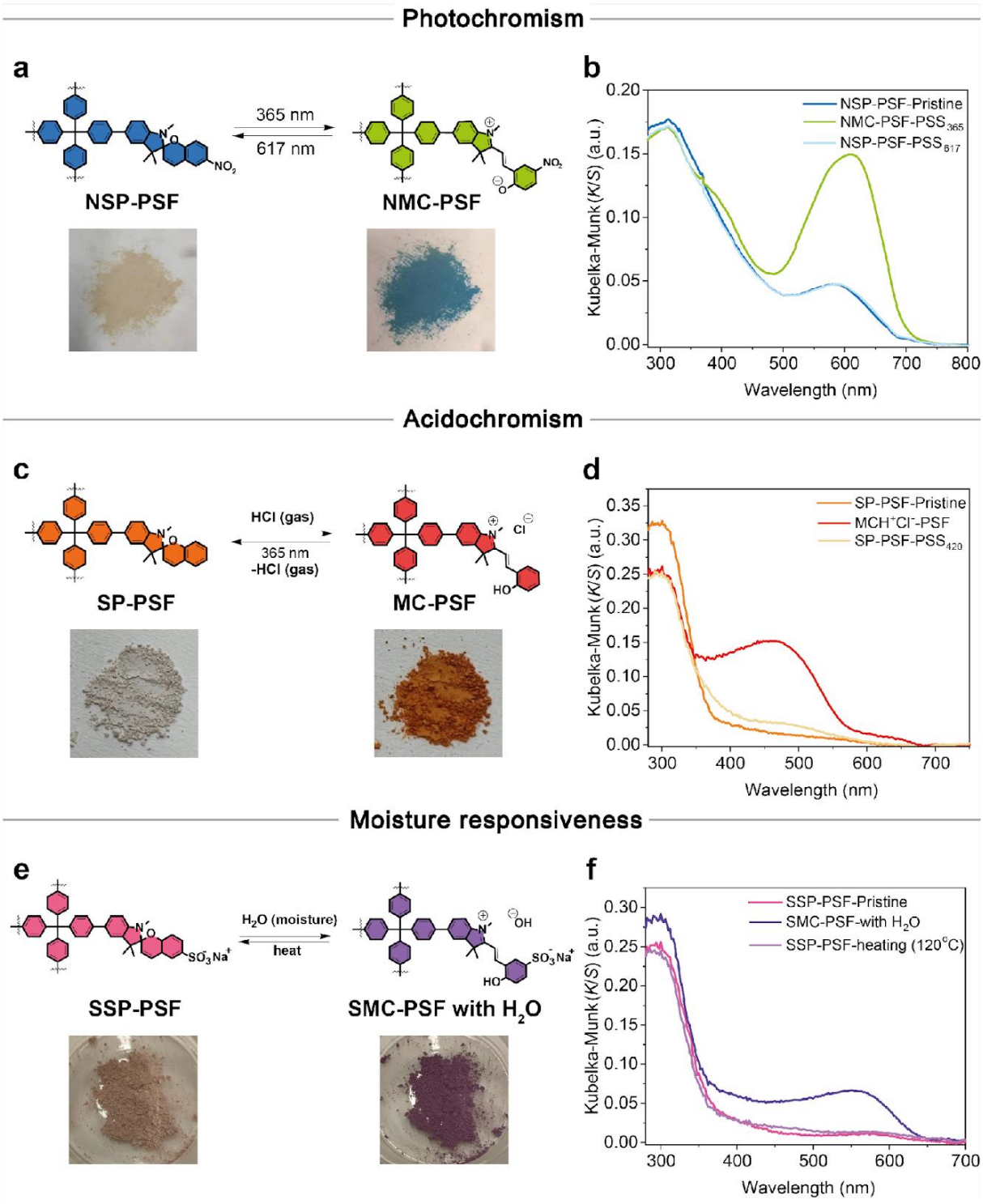

Figure 4. Multi-stimuli responsiveness of the **NSP-PSF**, **SP-PSF** and **SSP-PSF** materials. **a.** Schematic representation and visual changes of reversible photochromism of **NSP-PSF. b.** DR UV/Vis spectra showing the reversible photochromism of **NSP-PSF. c.** Schematic representation and visual changes of reversible acid-/photo- modulation of **SP-PSF. d.** DR UV/Vis

spectra of reversible acid-/photo- modulation of **SP-PSF. e.** Schematic representation and visual changes of reversible moisture/heat modulation of **SSP-PSF. f.** DR UV/Vis spectra of reversible moisture/heat modulation of **SSP-PSF.**

Multi-applications with SPs materials

To showcase the broad applicability of the PSF materials synthesized with this modular approach, a series of experiments testing the utility of these materials under various conditions were performed. Due to the large pore-capacity, **SP-PSF** could find potential applications as acidic gas sensor or sorbent that could be used to neutralize gas mixtures (Figure 5a). Indeed, when dry gaseous HCl was passed through the column packed with 10 mg of **SP-PSF** under N_2 flow, the dramatic color change from slight grey to deep orange was observed, indicating the formation of **MCH$^+$-PSF**. Subsequent irradiation at 365 nm on the column induced the release of the gaseous HCl in N_2 flow and therefore regeneration of the pristine **SP-PSF** material. The ultimate confirmation of this structural transformation upon $HCl_{(g)}$ exposure from the close to open form was provided by ^{13}C CP MAS NMR spectra which showed the acid-induced opening of the **SP-PSF** as demonstrated by the disappearance of the resonance characteristic of the SP isomer at 106.2 ppm (C_a, Figure 5b left) and the appearance of the new resonance at 182.3 ppm (C_a, Figure 5b, middle) characteristic of the MCH$^+$ form, further corroborated by an emergence of a single resonance corresponding the chemically equivalent methyl groups (C_e) in flat MC (Figure 5b, middle). Notably, the downfield resonance at 182.3 ppm is diagnostic of the formation of *E*-MCH$^+$ isomer.[53] Vice versa, after N_2-flow treatment the ^{13}C CP MAS NMR spectrum showed recovery of all the features of the closed form **SP-PSF** (Figure 5b, right). Thus, solid-state NMR spectroscopy highlights the quantitative (within the accuracy of the method) switching between the SP and the MCH$^+$ isomers, demonstrating the full accessibility of the SP switches decorating the pore surface. This process was followed by DR UV/Vis spectroscopy for two cycles which showed limited reversibility on account of the inhomogeneity in the gas flow and illumination of the material (Fig. S56). Nevertheless, this may be a question of experimental setup and in principle upon optimization of the setup this material can potentially be used as an acidic gas scavenger, which can be easily reactivated by light- and N_2-assisted acidic gas removal or when acidified as a release agent for acidic gas upon light irradiation.[66]

Due to the stability of the sulfonated MC form in polar media and the well-known capability of MC to bind metal ions, a metal ion binding experiment of the **SMC-PSF** material was investigated.[30] The **SSP-PSF** material was found to spontaneously undergo thermal isomerization to the open form in a highly-polar acetonitrile suspension. The presence of **SSP-PSF** in the $CuCl_2$ acetonitrile solution led to a significant drop of the adsorption at 460 nm, and a visible color change of the solid, showing the successful removal of Cu^{2+} from solution (Figure 5c, and Figure S57, grey spectrum). As observed from the UV/Vis spectra, the absorption band centered at 460 nm is related to the Cu^{2+} in acetonitrile. In contrast, the control solution without **SSP-PSF** showed much higher concentration of the Cu^{2+} (Figure

S57, orange spectrum), proving the ability of **SSP-PSF** material to remove Cu^{2+} and serve as a potential scavenger of transition-metal contaminants. Subsequent irradiation of the sample with visible light led to the release of the Cu^{2+} ions, corroborating the reversibility of the process.

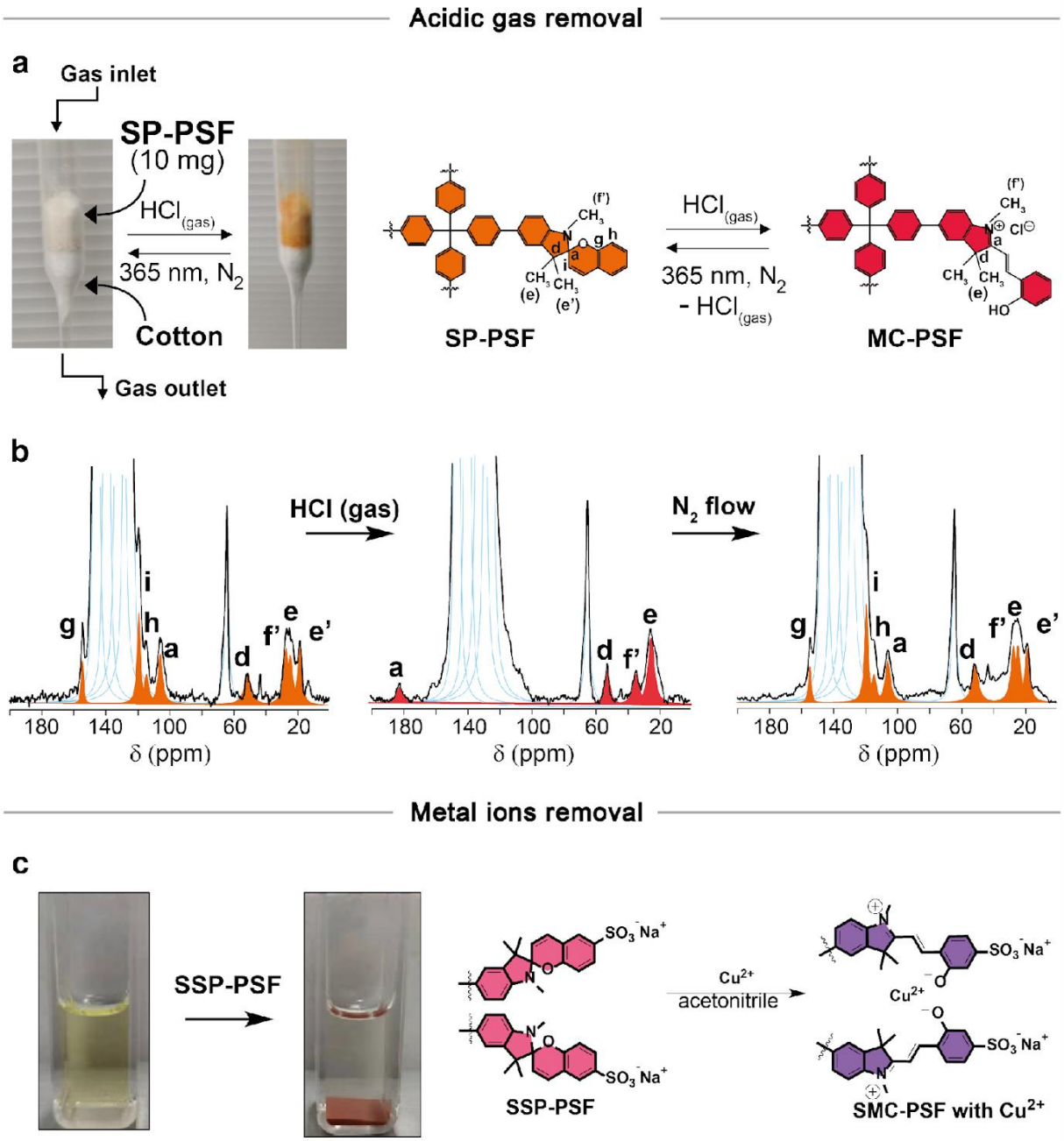

Figure 5. a. Demonstration of the reversible uptake and release of $HCl_{(g)}$ by **SP-PSF** material for acidic gas removal. **b.** $^{13}C\{^{1}H\}$ CP MAS spectra performed at 298 K at a spinning speed of 12.5 kHz with a contact time of 2 ms of pristine **SP-PSF** (left panel)**,** ***E*-MCH^{+}-PSF** (medium panel) and **SP-PSF** material (right panel) after complete regeneration under nitrogen flow. **c.** Demonstration of copper ion induced ring opening of **SSF-PSF** for metal ion capture.

Conclusion

In summary, by Yamamoto type cross-coupling reaction, an unprecedented indole-functionalized porous aromatic framework with ultra-high pore capacity in both micropore and mesopore region was

fabricated. Notably, the modular post-synthetic grafting to the pre-anchored indole sites allowed us to obtain SP functionalities as pendants in the nano-porous materials. Solid-state ^{13}C NMR confirmed the quantitative transformation of functionalities at each step during the solid-state synthesis and N_2 sorption data indicated the post-solid-state synthesis occurring in the entire framework without its collapse. Importantly, the high level of porosity maintained by this approach allows us to fabricate PSF based on SP, which is crucial for the responsive functions as well as capability of controlling material properties. It is worth to highlight that this is the first time that SP-based aromatic frameworks were constructed with remarkably high pore capacities. We furthermore demonstrate by DRUV-Vis, DRIFT spectroscopies and solid-state NMR studies, reversible photochromism of **NSP-PSF**, acidochromism of **SP-PSF** and **SSP-PSF**, ionochromism and humidity-responsiveness of **SSP-PSF**. The preservation of the multi-stimuli responsive behaviour of the SP in the constructed frameworks allowed us to show several areas in which these responsive materials can meet potential applications. Given the simplicity and efficiency of this modular synthetic approach, our work established an elegant strategy for the construction of highly porous yet chemically and structurally stable switchable materials with multi-stimuli responsive behavior. We also provide a more general synthesis strategy useful for other switchable materials with high pore capacity which cannot be accessed via *de novo* syntheses. Furthermore we envision that this strategy will allow to graft multiple functionalities within the same material, further increasing the functionality towards desired properties and applications. We are convinced that these switchable materials have potential to manifest more powerful functions beyond the examples illustrated herein transforming them into a crucial platform towards responsiveness and actuation on the molecular level in the solid state.

References

[1] B. L. Feringa, R. A. van Delden, N. Koumura, E. M. Geertsema, *Chem. Rev.* **2000**, *100*, 1789.
[2] W. R. Feringa, B. L. and Browne, *Molecular Switches*, Wiley-VCH Verlag GmbH & Co. KGaA, Weinheim, Germany, **2011**.
[3] Zbigniew L. Pianowski, *Molecular Photoswitches*, Wiley-VCH Verlag GmbH & Co. KGaA, Weinheim, Germany, **2022**.
[4] P. Theato, B. S. Sumerlin, R. K. O'reilly, T. H. Epp, *Chem. Soc. Rev.* **2013**, *42*, 7055.
[5] M. Wei, Y. Gao, X. Li, M. J. Serpe, *Polym. Chem.* **2017**, *8*, 127.
[6] A. Goulet-Hanssens, F. Eisenreich, S. Hecht, *Adv. Mater.* **2020**, *32*, 1905966.
[7] W. Danowski, T. Van Leeuwen, W. R. Browne, B. L. Feringa, *Nanoscale Adv.* **2021**, *3*, 24.
[8] Y. Yin, J. A. Rogers, *Chem. Rev.* **2022**, *122*, 4885.
[9] G. Berkovic, V. Krongauz, V. Weiss, *Chem. Rev.* **2000**, *100*, 1741.
[10] F. Xu, B. L. Feringa, *Adv. Mater.* **2023**, *35*, 2204413.
[11] S. Swansburg, E. Buncel, R. P. Lemieux, *J. Am. Chem. Soc.* **2000**, *122*, 6594.
[12] V. I. Minkin, *Chem. Rev.* **2004**, *104*, 2751.
[13] L. Kortekaas, W. R. Browne, *Chem. Soc. Rev.* **2019**, *48*, 3406.
[14] M. Li, Q. Zhang, Y.-N. Zhou, S. Zhu, *Prog. Polym. Sci.* **2018**, *79*, 26.
[15] R. Klajn, *Chem. Soc. Rev.* **2014**, *43*, 148.
[16] A. Coskun, M. Banaszak, R. D. Astumian, J. F. Stoddart, B. A. Grzybowski, *Chem. Soc. Rev.* **2012**, *41*, 19.
[17] J. Keyvan Rad, Z. Balzade, A. R. Mahdavian, *J. Photochem. Photobiol. C Photochem. Rev.* **2022**,

51, 100487.
[18] C. Li, A. Iscen, H. Sai, K. Sato, N. A. Sather, S. M. Chin, Z. Álvarez, L. C. Palmer, G. C. Schatz, S. I. Stupp, *Nat. Mater.* **2020**, *19*, 900.
[19] L. Kortekaas, O. Ivashenko, J. T. van Herpt, W. R. Browne, *J. Am. Chem. Soc.* **2016**, *138*, 1301.
[20] W. Francis, A. Dunne, C. Delaney, L. Florea, D. Diamond, *Sensors Actuators, B Chem.* **2017**, *250*, 608.
[21] A. Meeks, M. M. Lerch, T. B. H. Schroeder, A. Shastri, J. Aizenberg, *J. Am. Chem. Soc.* **2022**, *144*, 219.
[22] D. R. Morim, A. Meeks, A. Shastri, A. Tran, A. V. Shneidman, V. V. Yashin, F. Mahmood, A. C. Balazs, J. Aizenberg, K. Saravanamuttu, *Proc. Natl. Acad. Sci.* **2020**, *117*, 3953.
[23] C. Li, A. Iscen, L. C. Palmer, G. C. Schatz, S. I. Stupp, *J. Am. Chem. Soc.* **2020**, *142*, 8447.
[24] Y. J. Jeong, E. J. Yoo, L. H. Kim, S. Park, J. Jang, S. H. Kim, S. W. Lee, C. E. Park, *J. Mater. Chem. C* **2016**, *4*, 5398.
[25] O. Ivashenko, J. T. van Herpt, B. L. Feringa, P. Rudolf, W. R. Browne, *Langmuir* **2013**, *29*, 4290.
[26] J. Cao, S. Wu, B. Zhai, Q. Wang, J. Li, X. Ma, *Dye. Pigment.* **2014**, *103*, 89.
[27] Y. Zhang, M. Ng, E. Y.-H. Hong, A. K.-W. Chan, N. M.-W. Wu, M. H.-Y. Chan, L. Wu, V. W.-W. Yam, *J. Mater. Chem. C* **2020**, *8*, 13676.
[28] S. Kwangmettatam, T. Kudernac, *Chem. Commun.* **2018**, *54*, 5311.
[29] A. Koçer, M. Walko, W. Meijberg, B. L. Feringa, *Science* . **2005**, *309*, 755.
[30] P. K. Kundu, G. L. Olsen, V. Kiss, R. Klajn, *Nat. Commun.* **2014**, *5*, 3588.
[31] D. E. Williams, C. R. Martin, E. A. Dolgopolova, A. Swifton, D. C. Godfrey, O. A. Ejegbavwo, P. J. Pellechia, M. D. Smith, N. B. Shustova, *J. Am. Chem. Soc.* **2018**, *140*, 7611.
[32] E. A. Dolgopolova, V. A. Galitskiy, C. R. Martin, H. N. Gregory, B. J. Yarbrough, A. M. Rice, A. A. Berseneva, O. A. Ejegbavwo, K. S. Stephenson, P. Kittikhunnatham, S. G. Karakalos, M. D. Smith, A. B. Greytak, S. Garashchuk, N. B. Shustova, *J. Am. Chem. Soc.* **2019**, *141*, 5350.
[33] A. B. Kanj, A. Chandresh, A. Gerwien, S. Grosjean, S. Bräse, Y. Wang, H. Dube, L. Heinke, *Chem. Sci.* **2020**, *11*, 1404.
[34] S. Garg, H. Schwartz, M. Kozlowska, A. B. Kanj, K. Müller, W. Wenzel, U. Ruschewitz, L. Heinke, *Angew. Chem. Int. Ed.* **2019**, *58*, 1193.
[35] H. Liang, Y. Guo, Y. Shi, X. Peng, B. Liang, B. Chen, *Angew. Chem. Int. Ed.* **2020**, *59*, 7732.
[36] R. Ou, H. Zhang, V. X. Truong, L. Zhang, H. M. Hegab, L. Han, J. Hou, X. Zhang, A. Deletic, L. Jiang, G. P. Simon, H. Wang, *Nat. Sustain.* **2020**, *3*, 1052.
[37] C. R. Martin, K. C. Park, G. A. Leith, J. Yu, A. Mathur, G. R. Wilson, G. B. Gange, E. L. Barth, R. T. Ly, O. M. Manley, K. L. Forrester, S. G. Karakalos, M. D. Smith, T. M. Makris, A. K. Vannucci, D. V. Peryshkov, N. B. Shustova, *J. Am. Chem. Soc.* **2022**, *144*, 4457.
[38] G. C. Thaggard, G. A. Leith, D. Sosnin, C. R. Martin, K. C. Park, M. K. McBride, J. Lim, B. J. Yarbrough, B. K. P. Maldeni Kankanamalage, G. R. Wilson, A. R. Hill, M. D. Smith, S. Garashchuk, A. B. Greytak, I. Aprahamian, N. B. Shustova, *Angew. Chem. Int. Ed.* **2023**, *62*, e202211776.
[39] C. R. Martin, G. A. Leith, P. Kittikhunnatham, K. C. Park, O. A. Ejegbavwo, A. Mathur, C. R. Callahan, S. L. Desmond, M. R. Keener, F. Ahmed, S. Pandey, M. D. Smith, S. R. Phillpot, A. B. Greytak, N. B. Shustova, *Angew. Chem. Int. Ed.* **2021**, *60*, 8072.
[40] A. B. Grommet, L. M. Lee, R. Klajn, *Acc. Chem. Res.* **2020**, *53*, 2600.
[41] K. Healey, W. Liang, P. D. Southon, T. L. Church, D. M. D'Alessandro, *J. Mater. Chem. A* **2016**, *4*, 10816.
[42] S. Shi, K.-D. Li, Y.-X. Li, Z.-D. Ma, S.-C. Qi, X.-Q. Liu, L.-B. Sun, *ACS Mater. Lett.* **2023**, *5*, 2189.
[43] G. Das, T. Prakasam, N. Alkhatib, R. G. AbdulHalim, F. Chandra, S. K. Sharma, B. Garai, S. Varghese, M. A. Addicoat, F. Ravaux, R. Pasricha, R. Jagannathan, N. Saleh, S. Kirmizialtin, M. A. Olson, A. Trabolsi, *Nat. Commun.* **2023**, *14*, 3765.
[44] T. Ben, H. Ren, S. Ma, D. Cao, J. Lan, X. Jing, W. Wang, J. Xu, F. Deng, J. M. Simmons, S. Qiu, G. Zhu, *Angew. Chem. Int. Ed.* **2009**, *48*, 9457.
[45] D. Yuan, W. Lu, D. Zhao, H. C. Zhou, *Adv. Mater.* **2011**, *23*, 3723.
[46] F. Castiglioni, W. Danowski, J. Perego, F. K. C. Leung, P. Sozzani, S. Bracco, S. J. Wezenberg, A. Comotti, B. L. Feringa, *Nat. Chem.* **2020**, *12*, 595.

[47] J. Sheng, W. Danowski, S. Crespi, A. Guinart, X. Chen, C. Stähler, B. L. Feringa, *Chem. Sci.* **2023**, *14*, 4328.
[48] J. Schmidt, M. Werner, A. Thomas, *Macromolecules* **2009**, *42*, 4426.
[49] R. Delgado-Macuil, M. Rojas-López, V. L. Gayou, A. Orduña-Díaz, J. Díaz-Reyes, *Mater. Charact.* **2007**, *58*, 771.
[50] R. M. Silverstein, G. C. Bassler, *J. Chem. Educ.* **1962**, *39*, 546.
[51] A. Comotti, S. Bracco, M. Mauri, S. Mottadelli, T. Ben, S. Qiu, P. Sozzani, *Angew. Chem. Int. Ed.* **2012**, *51*, 10136.
[52] T. Halbritter, C. Kaiser, J. Wachtveitl, A. Heckel, *J. Org. Chem.* **2017**, *82*, 8040.
[53] L. Wimberger, S. K. K. Prasad, M. D. Peeks, J. Andréasson, T. W. Schmidt, J. E. Beves, *J. Am. Chem. Soc.* **2021**, *143*, 20758.
[54] Y. Xu, J. Fei, G. Li, T. Yuan, Y. Li, C. Wang, X. Li, J. Li, *Angew. Chem.* **2017**, *129*, 13083.
[55] C. Li, Y. Xue, M. Han, L. C. Palmer, J. A. Rogers, Y. Huang, S. I. Stupp, *Matter* **2021**, *4*, 1377.
[56] M. Reifarth, M. Bekir, A. M. Bapolisi, E. Titov, F. Nußhardt, J. Nowaczyk, D. Grigoriev, A. Sharma, P. Saalfrank, S. Santer, M. Hartlieb, A. Böker, *Angew. Chem. Int. Ed.* **2022**, *61*, e202114687.
[57] J. Ma, J. Tian, Z. Liu, D. Shi, X. Zhang, G. Zhang, D. Zhang, *CCS Chem.* **2020**, *2*, 632.
[58] J. Perego, D. Piga, S. Bracco, P. Sozzani, A. Comotti, *Chem. Commun.* **2018**, *54*, 9321.
[59] W. Lu, D. Yuan, J. Sculley, D. Zhao, R. Krishna, H.-C. Zhou, *J. Am. Chem. Soc.* **2011**, *133*, 18126.
[60] L. Kortekaas, J. Chen, D. Jacquemin, W. R. Browne, *J. Phys. Chem. B* **2018**, *122*, 6423.
[61] D. Moldenhauer, F. Gröhn, *Chem. - A Eur. J.* **2017**, *23*, 3966.
[62] N. Hanikel, M. S. Prévot, O. M. Yaghi, *Nat. Nanotechnol.* **2020**, *15*, 348.
[63] W. Xu, O. M. Yaghi, *ACS Cent. Sci.* **2020**, *6*, 1348.
[64] H. L. Nguyen, N. Hanikel, S. J. Lyle, C. Zhu, D. M. Proserpio, O. M. Yaghi, *J. Am. Chem. Soc.* **2020**, *142*, 2218.
[65] H. L. Nguyen, C. Gropp, N. Hanikel, A. Möckel, A. Lund, O. M. Yaghi, *ACS Cent. Sci.* **2022**, 8, 926.
[66] H. Bamdad, K. Hawboldt, S. MacQuarrie, *Renew. Sustain. Energy Rev.* **2018**, *81*, 1705.

ORCID

Jinyu Sheng: 0000-0001-8141-9089

Jacopo Perego: 0000-0003-4795-2060

Silvia Bracco: 0000-0002-2575-6424

Wojciech Danowski: 0000-0002-8588-8912

Simon Krause: 0000-0001-9504-8514

Piero Sozzani: 0000-0002-5981-4039

Artur Ciesielski: 0000-0003-3542-4092

Angiolina Comotti: 0000-0002-8396-8951

Ben L. Feringa: 0000-0003-0588-8435

Conflict of Interest:

There are no competing conflicts of interests to declare.

Acknowledgements

This work was supported from the following sources: China Scholarship Council (CSC PhD Fellowship No. 201808330459 to J.S.), Financial support from The Netherlands Organization for Scientific Research (NWO-CW), the European Research Council (ERC; advanced Grant No. 694345 to B.L.F.). The Ministero dell'Istruzione, dell'Università, PRIN (SHERPA) and Lombardy Region for "Enhancing Photosynthesis" grant (2021-2023) are acknowledged for the financial support. W.D. is grateful for financial support from Marie Skłodowska-Curie Actions (Individual Fellowship No. 101027639). We thank prof. Wesley R. Browne for fruitful discussions.

Author contributions

J.S. and B.L.F. conceived the project. B.L.F., P.S. and A.C. guided and supervised the research. J.S. synthesized the building blocks and all materials. J.S. carried out the UV and NMR irradiation studies in solution and DR-UV-vis and FT-IR measurements in solid state. J.S. carried out the SEM measurements, J.P. performed thermogravimetric analysis, elemental analysis, solid state irradiation, gas adsorption isotherms. S.K. supported sample activation and adsorption analysis. S.B. carried solid state irradiation and solid state NMR spectra. J.S., W.D., J.P., P.S. and A.C. wrote the manuscript with contributions from all coauthors. All of the authors participated in the discussion of data and commented on the manuscript.